Published in final edited form as:
Nat Cell Biol. 2009 June ; 11(6): 705–716. doi:10.1038/ncb1876.

A functional screen implicates microRNA-138-dependent regulation of the depalmitoylation enzyme APT1 in dendritic spine morphogenesis

Gabriele Siegel[1,11], **Gregor Obernosterer**[2,11], **Roberto Fiore**[1], **Martin Oehmen**[3], **Silvia Bicker**[1], **Mette Christensen**[1,4], **Sharof Khudayberdiev**[1], **Philipp F. Leuschner**[2], **Clara J. L. Busch**[2], **Christina Kane**[5], **Katja Hübel**[6], **Frank Dekker**[6], **Balamurugan Rengarajan**[6], **Carsten Drepper**[7,9], **Herbert Waldmann**[6], **Sakari Kauppinen**[4,8], **Michael E. Greenberg**[5], **Andreas Draguhn**[3], **Marc Rehmsmeier**[7,10], **Javier Martinez**[2,*], and **Gerhard M. Schratt**[1,**]

[1]Interdisziplinäres Zentrum für Neurowissenschaften, SFB488 Junior Group, Universität Heidelberg, and Institut für Neuroanatomie, Universitätsklinikum Heidelberg, Im Neuenheimer Feld 345, 69120 Heidelberg, Germany

[2]Institute of Molecular Biotechnology, IMBA, Austrian Academy of Sciences, Dr. Bohr Gasse 3, 1030 Vienna, Austria

[3]Institut für Physiologie und Pathophysiologie, Universität Heidelberg, Im Neuenheimer Feld 326, 69120 Heidelberg, Germany

[4]Wilhelm Johannsen Center for Functional Genome Research, Department of Cellular and Molecular Medicine, University of Copenhagen, Blegdamsvej 3, DK-2200 Cph N, Denmark

[5]Department of Neurobiology, Harvard Medical School, 220 Longwood Avenue, Boston, MA 02115, USA

[6]Max-Planck-Institut für molekulare Physiologie, Abteilung Chemische Biologie, and Technische Universität Dortmund, Fakultät Chemie, Chemische Biologie, Otto-Hahn-Str. 11, 44227 Dortmund, Germany

[7]Center for Biotechnology (CeBiTec), Universität Bielefeld, 33594 Bielefeld, Germany

[8]Santaris Pharma, Boege Alle 3, DK-2970 Hoersholm, Denmark

Summary

The microRNA pathway has been implicated in the regulation of synaptic protein synthesis and ultimately dendritic spine morphogenesis, a phenomenon associated with long-lasting forms of memory. However, the particular microRNAs (miRNAs) involved are largely unknown. We performed a functional screen to identify specific miRNAs that function at synapses to control dendritic spine structure. One of the identified miRNAs, miR-138, is highly enriched in the brain, localized within dendrites and negatively regulates the size of dendritic spines in rat hippocampal neurons. miR-138 controls the expression of Acyl protein thioesterase 1 (APT1), an enzyme regulating the palmitoylation status of proteins that are known to function at the synapse, including G protein alpha subunits (Gα). RNAi-mediated knockdown of APT1 and expression of membrane-localized Gα both suppress spine enlargement caused by miR-138 inhibition,

[*]corresponding author: javier.martinez@imba.oeaw.ac.at. [**]corresponding author: schratt@ana.uni-heidelberg.de.
[9]present address: Institute for Clinical Neurobiology, ZEMM, Zinklesweg 10, Wuerzburg University, 97078 Würzburg, Germany
[10]present address: Gregor Mendel Institute of Molecular Plant Biology, Dr. Bohr-Gasse 3, 1030 Vienna, Austria
[11]These authors contributed equally to this work.

The authors declare that they have no competing financial interest.

suggesting that APT1-regulated depalmitoylation of Gα might be an important downstream event of miR-138 function. Our results uncover a novel miRNA-dependent mechanism in neurons and demonstrate a previously unrecognized complexity of miRNA-dependent control of dendritic spine morphogenesis.

Introduction

The functioning of the mammalian brain relies on the proper formation of intricate neuronal circuits. Neurons within these circuits are synaptically connected, and the majority of excitatory synaptic connections between neurons form on dendritic spines, specialized protrusions emanating from the dendritic shaft [1, 2]. The structural and functional plasticity of dendritic spines correlates with long-lasting changes in synaptic transmission that underlie higher cognitive functions [3, 4]. Dendritic spine abnormalities are a hallmark of a variety of neurological diseases, including several forms of mental retardation [5]. A plethora of molecular mechanisms involved in dendritic spine plasticity has been elucidated during the last decade, including actin cytoskeletal dynamics, post-translational protein modifications, protein trafficking, gene transcription and protein turnover [6–10]. The de-novo synthesis of proteins is of particular importance for enduring changes in synaptic transmission that are associated with long-term memory [11, 12]. Proteins can be either synthesized in the soma and transported to dendritic spines, or they can be locally synthesized from a pool of dendritic mRNAs within or next to spines [13–15].

The local translation of dendritic mRNAs is regulated tightly by RNA-binding proteins and non-coding RNAs that preferentially bind to the 3' untranslated region (UTR) of the mRNAs [16, 17]. miRNAs, a diverse class of 20–24 nucleotide non-coding RNAs, regulate local mRNA translation in dendrites, thereby affecting the morphology of dendritic spines in rat hippocampal neurons [18, 19].

miRNAs are expressed in basically all cell types and regulate important biological processes, including differentiation, apoptosis, and cellular transformation [20, 21]. miRNAs inhibit mRNA translation by binding to cognate sites in the 3'UTR of target mRNAs [22]. In the mammalian nervous system, miRNAs function during cell specification (miR-124a, miR-9), neurite outgrowth (miR-132) and spine development (miR-134) [23]. Microarray and cloning experiments demonstrate that a large number of miRNAs is expressed in the postnatal mammalian brain at times of synapse development, but their role in synapse formation and plasticity is largely unknown [24–26]. Here we present a functional screen that led to the identification of miRNAs that are involved in dendritic spine morphogenesis. Among these miRNAs, miR-138 was found to robustly inhibit the growth of dendritic spines, an effect that was mediated by downregulation of APT1, an enzyme catalyzing the depalmitoylation of a number of signaling proteins [27]. Our findings define a novel mechanism by which miRNAs control dendritic spine morphogenesis and point to a hitherto unrecognized complexity of miRNA function in the regulation of synaptic plasticity in mammalian neurons.

Results

Large-scale identification of synaptically enriched miRNAs

To identify miRNAs that function during synaptic development, we undertook a combination of expression profiling of miRNAs in the synaptodendritic compartment and subsequent functional inhibitory screening in primary hippocampal neurons. We reasoned that miRNAs that are important for synapse function might primarily reside near the synapse, where they could locally regulate the translation of critical target mRNAs.

Synaptosomes, a biochemical fraction highly enriched for synaptic membranes, preserve components of local protein synthesis, including polyribosomes, mRNAs and regulatory RNAs ([28], Figure 1A and data not shown). We therefore conclude that synaptosomes represent a suitable source for synaptic miRNAs. Total RNA was extracted from P15 rat forebrains and synaptosomes and simultaneously hybridized to microarrays that contained probes for all mouse and rat mature miRNAs listed in the Sanger database (miRBase, version 7.1, http://www.sanger.ac.uk/Software/Rfam/mirna/). Thereby, we identified a list of 10 mature miRNAs that displayed an at least twofold enrichment in synaptosomes compared to whole forebrain in three biological replicates. Conversely, four mature miRNAs were strongly depleted from synaptosomes (Fig. 1B, C).

The observed enrichment of several miRNAs in RNA preparations from synaptosomes was validated for selected candidates by Northern blot analysis (Fig. 2A). In accordance with the microarray data, we found higher levels of miR-218 (3.02-fold) and miR-138 (1.67-fold) in total RNA prepared from synaptosomes compared to whole forebrain. In contrast, mature miR-124 was not enriched (0.97-fold) and pre-miR-124 was undetectable in synaptosomes, confirming that only specific miRNAs are enriched at the synapse.

To monitor the subcellular localization of miRNAs identified in our screen, we performed *in situ* hybridization (ISH) in rat hippocampal neurons at 18 days *in vitro* (DIV) (Fig. 2B), using probes for miR-9, miR-218, miR-138 and miR-124 as a control (Fig. 2A, Suppl. Table 1). All candidate miRNAs were readily detected in cultured hippocampal neurons using locked nucleic acid (LNA) oligonucleotides as detection probes. We confirmed the specificity of our ISH protocol by using a scrambled LNA control oligonucleotide (Fig. 2B, upper left panel). Neuronal expression of miR-138 was further confirmed by ISH in brain slices (Suppl. Fig. 1A,B), quantitative RT-PCR and Northern blotting using RNA from dissociated primary neurons (Suppl. Fig. 1A-D). Whereas miR-124 was mainly localized within the cell body (Fig. 1B, asterisks), the signals for miR-138, miR-218 and miR-9 extended well into neuronal processes that were identified as dendrites by co-staining for the dendritic marker protein MAP2 (Fig. 2B, arrowheads). Quantification of the ISH signals (Fig. 2B, lower right panel) confirmed the enrichment of miR-138, miR-218 and miR-9 in dendrites relative to the cell body restricted miR-124. Taken together, our microarray, Northern blot and ISH data demonstrated that a specific subset of miRNAs is enriched in the synaptodendritic compartment of rat neurons. These findings suggest the existence of a dendritic miRNA regulatory network.

Functional screening identifies miR-138 as a negative regulator of dendritic spine size

To study the functional relevance of the miRNA regulatory network in dendrites, we interfered with the function of candidate miRNAs identified in the microarray analysis by transfecting cells with miRNA antagonists (2'-O-methyl (2'O-me) modified antisense (AS) oligoribonucleotides) [29]. We hypothesized that some of the miRNAs identified in the screen might affect dendritic spine morphology, a correlate of the maturity and strength of excitatory synapses [3, 4, 30] (Figure 3A).

Using a single cell fluorescent sensor assay [31], we found that transfection of 2'O-me AS oligos significantly reduced miRNA-mediated sensor cleavage for three selected miRNAs (miR-138, miR-132, miR-218) that are endogenously expressed in hippocampal neurons (10–18 DIV, Suppl. Fig. 1E). Therefore, 2'O-me AS oligos are suitable to achieve specific inhibition of individual miRNAs. We analyzed candidate miRNAs that displayed an at least two-fold enrichment in synaptosomes compared to whole brain. In addition, miR-132 was included since it regulates dendritic outgrowth [32]. Inhibition of miRNA function by 2'O-me AS oligonucleotides resulted in a significant change in dendritic spine volume for two of the miRNAs tested, miR-138 and miR-132, when compared to control transfected neurons (Fig.

3B). Inhibition of miR-138 function resulted in a robust and significant increase in spine volume (Fig. 3B, C) without altering the total number of synaptic puncta (Suppl. Fig. 2A). Introducing 2'O-me AS oligonucleotides directed against the other nine candidate miRNAs or three control sequences (2'O-me control, 2'O-me let7c, 2'O-me 126) did not significantly affect spine volume (Fig. 3B), demonstrating that we can specifically interfere with dendritic spine morphogenesis.

Since miR-138 inhibition very robustly changed dendritic spine size, and the role of miR-138 in the nervous system and synaptic development were completely unknown, we decided to focus on miR-138. To further corroborate our findings, we employed another AS oligonucleotide inhibitor of different chemistry (locked nucleic acids, LNA). Similar to 2'-O-me 138, transfection of LNA-138 specifically increased the average spine volume of hippocampal neurons (Fig. 3D). Conversely, transfection of miR-138 duplex RNA significantly decreased average spine volume, supporting an inhibitory role for miR-138 in spine growth (Fig. 3E). miR-138 duplex RNA, but not a control RNA (let-7c), was able to completely revert the spine-growth promoting effect observed upon miR-138 inhibition, demonstrating the specificity of the effect on spine size (Fig. 3F). Overexpression of either duplex RNA had no significant effect on dendritic spine density or the dendritic branching index (Suppl. Fig. 2B-C), indicating that overall dendritic morphology was not compromised by the introduction of synthetic small RNAs.

Therefore, we identified miR-138 as a critical component of a regulatory pathway that orchestrates dendritic spine growth. Calcium influx into cortical neurons as induced by membrane depolarization led to a rapid and progressive decline of pre-miR-138 expression (Suppl. Fig. 2D) and miR-138 cleavage activity (Suppl. Fig. 2E), indicating that miR-138 could be regulated during activity-dependent spine development.

miR-138 regulates synaptic transmission and AMPAR surface staining

We next asked whether the observed changes in spine morphology upon miR-138 perturbation are associated with corresponding alterations in excitatory synaptic function. We recorded miniature excitatory postsynaptic currents (mEPSC; Fig. 4A) from cultured hippocampal neurons that had been transfected with miR-138, control duplex RNA, or with a vector expressing GFP only. In miR-138 expressing neurons, the median amplitude of mEPSCs was significantly reduced compared to both control transfections (Fig. 4B,C). Frequency of events was not different between all three types of cells. This result is consistent with our previous observations that miR-138 expression leads to a 25% decrease in spine volume (Fig. 3D), but has no effect on spine density (Suppl. Fig. 2B). Miniature EPSCs were sensitive to CNQX and were therefore largely mediated by AMPARs (data not shown). Accordingly, we found a reduction in the median size, but not density, of GluR2-containing AMPAR clusters in dendrites of miR-138 expressing neurons (Fig. 4D and data not shown, KS-test <0.001). Thus, miR-138 mediated spine shrinkage correlates with a decrease in the amplitude of postsynaptic currents and AMPAR cluster size.

Acyl-protein thioesterase (APT1) mRNA is a miR-138 target in neurons

Using the RNAhybrid program we predicted miR-138 target mRNAs that might mediate the miR-138 effect on spine morphogenesis [33, 34]. We selected four putative miR-138 target mRNAs that appeared to be particularly interesting in terms of synaptic function: EphrinB3 [35], PLEKHB1 [36], RIMS2 [37] and APT1 [38].

To validate the functionality of the identified binding sites within these mRNAs, full-length 3'UTRs of the candidate miR-138 targets were cloned downstream of the luciferase coding region and these constructs were transfected into cortical neurons along with miR-138

duplex RNA. The APT1 3'UTR conferred the most robust reduction in luciferase activity upon miR-138 cotransfection in both HeLa cells that lack endogenous miR-138 and primary neurons (Fig. 5A, Suppl. Fig. 3A). Hence, we decided to focus on APT1 and study its regulation by miR-138 in more detail.

Introduction of miR-138 into cortical neurons did not significantly alter steady-state APT1-luciferase mRNA levels (Suppl. Fig. 3B), suggesting that the inhibitory effect of miR-138 on APT1 expression is mainly due to impaired APT1 mRNA translation. APT1 (Acyl protein thioesterase 1) catalyzes the removal of palmitate, a lipid modification which plays important roles in the localization and function of proteins [39]. Expression and function of APT1 in the nervous system were completely unknown, but the fact that dynamic palmitoylation of synaptic proteins has been implicated in the regulation of synaptic efficacy [40] made APT1 an interesting candidate in the context of dendritic spine morphology. To test for the physiological significance of the miR-138 APT1 interaction, we explored the expression of APT1 mRNA and protein using brain slices and isolated primary neurons. By ISH, mouse APT1 mRNA was detected in multiple brain regions, including the principal layers of the hippocampus (Fig. 5B, data not shown). In hippocampal neurons, APT1 mRNA localized to the somatic and dendritic compartment (Fig. 5C). Similar to the known dendritic mRNA MAP2, APT1 mRNA was concentrated in granule-like structures along the length of dendrites (Fig. 5D). APT1 protein gradually increased over three weeks of cortical neuron development *in vitro* (Fig. 5E). At the subcellular level, APT1 protein was present in both the cytosolic (S1, S2) and membranous fractions (P2, SYN) of P15 rat brain (Fig. 5F). However, in contrast to PSD-95, the majority of APT1 protein accumulated in the soluble cytosolic fractions. These results are consistent with the idea that at least part of the negative regulatory interaction between miR-138 and APT1 mRNA occurs locally in the synaptodendritic compartment.

We next tested whether the predicted miR-138 binding site within the APT1 3'UTR is sufficient for miR-138 mediated translational inhibition. The duplex between the target site of the APT1 3'UTR and miR-138 features extensive complementarity, especially within a highly conserved region at the 5' end of the miRNA known as the "seed" region (Fig. 6A). Accordingly, point mutations within this seed region (APT1 mutant) rendered the APT1-luciferase construct insensitive to miR-138 mediated inhibition (Fig. 6B). Therefore, inhibition of APT1 expression by miR-138 is mediated via a single conserved miR-138 binding site within the APT1 3'UTR. To test whether endogenous miR-138 regulates the translation of APT1 mRNA in neurons, we transfected the APT1-luciferase reporter into mature, miR-138 expressing neurons (14-16 DIV; Fig. 6C). Inhibition of endogenous miR-138 by 2'O-me-138 specifically upregulated APT1-luciferase expression in a dose-dependent manner. This inhibitory function of endogenous miR-138 on the APT1 reporter construct was dependent on a functional miR-138 binding site (Fig. 6C, suppl. Fig. 3C). The effect of 2'O-me-138 on APT1 expression was specific, since it was effectively competed for by the transfection of miR-138 duplex RNA (suppl. Fig. 3D). Quantitative transduction of primary neurons by bath application of cholesterol-modified 2'O-me-138 led to a reproducible and specific upregulation of APT1 protein as assessed by semi-quantitative Western blotting (Fig. 6D). In summary, our results establish APT1 as a bona fide miR-138 target mRNA, thereby implicating miR-138 in the regulation of palmitoylation in neurons.

APT1 activity is required for spine enlargement caused by miR-138 inhibition

We next explored whether the reduction in dendritic spine volume upon miR-138 overexpression might be causally linked to decreased APT1 expression. First, we monitored spine volume in neurons in which endogenous APT1 levels were reduced by RNAi. As judged by Western blotting, three out of four APT1 small hairpin RNAs (shRNAs) targeting different regions of the APT1 mRNA effectively reduced endogenous APT1 protein in

cortical neurons (Figure 7A, Suppl. Fig. 4B) and ectopically expressed APT1 in HEK293 cells (Suppl. Fig. 4A). In hippocampal neurons, APT1 knockdown by each of the effective shRNAs (APT1 shRNA-1, -3 and -4) led to a significant reduction in the size of dendritic protrusions compared to control conditions (Figure 7B, C, and data not shown). Reduced spine volume upon APT1 knockdown was accompanied by a significant reduction in the number of spine-associated PSD-95 clusters within dendrites (Suppl. Fig. 4C-E). None of the APT1 shRNAs had an effect on the total number of dendritic protrusions of hippocampal neurons (Suppl. Fig. 5A) or the dendritic branching index (Suppl. Fig. 5B), indicating a specific effect of APT1 knockdown on spine morphology. APT1-dependent control of dendritic spine morphology required APT1 depalmitoylating activity, since inhibition of APT1 enzymatic activity by two different small molecule inhibitors (FD196, FD253) similarly led to a reduction in dendritic spine volume (Figure 7D and Suppl. Fig. 5C), whereas an inactive control compound (RB020) had no effect.

We next tested whether elevated APT1 levels caused by miR-138 inhibition are required for the increase in spine volume. Reduction of APT1 levels by APT1 shRNA-3 in miR-138-depleted cells completely suppressed the spine growth promoting effect of miR-138 inhibition by 2'-Ome 138 (Fig. 7E) and LNA-138 (Suppl. Fig. 5D). Conversely, transfection of an APT1 expression construct harboring a mutation in the miR-138 binding site (APT1 mutBS), but not a wild-type APT1 construct, efficiently rescued spine shrinkage caused by elevated miR-138 levels (Fig. 7F). Together, these two lines of evidence strongly suggest that APT1 is a critical downstream effector of miR-138 in the regulation of spine morphogenesis.

Membrane localization of the APT1 substrate G protein α 13 (Gα13) counteracts spine enlargement caused by miR-138 inhibition

We investigated the molecular mechanism that underlies dendritic spine enlargement caused by increased APT1 protein levels upon miR-138 inhibition. APT1 depalmitoylates a number of substrates implicated in synaptic plasticity, including endothelial nitric oxide synthase (eNOS), H-Ras and G protein α (Gα) subunits, i.e. Gα13 [27]. Since Gα13 palmitoylation is required for plasma membrane localization and Rho-dependent signaling [41], we focused on Gα13. We found that a significant fraction of overexpressed myc-Gα13 re-distributes from the cytosol to the membrane upon shRNA-mediated knockdown of endogenous hAPT1 in HEK293 cells (Figure 8A-C). In contrast, transfection of an APT1 expression construct (CFP-APT1) had the opposite effect. Thus, APT1 is necessary and sufficient for Gα13 membrane localization in HEK293 cells, presumably via Gα13 depalmitoylation. More importantly, introduction of synthetic miR-138 duplex RNA similarly increases membrane association of myc-Gα13 (Fig. 8D, E). miR-138 had no effect on the subcellular distribution of the cytosolic beta-actin or membrane-associated calnexin proteins (Fig. 8D). Gα13 redistribution coincides with a reduction in endogenous hAPT1 protein levels in miR-138 transfected HEK293 cells (Fig. 8F).

Finally, we investigated the significance of the regulation of Gα subcellular localization by miR-138 for the control of spine size. Similar to APT1 knockdown (Fig. 7F), overexpression of wild-type Gα13 was able to suppress the spine growth promoting effect caused by miR-138 inhibition (Fig. 8G). A palmitoylation deficient Gα13 (Gα13 CCSS) was ineffective in the rescue experiment, demonstrating that Gα palmitoylation is required for miR-138-mediated spine shrinkage. The effects of Gα13 palmitoylation are likely due to redistribution of Gα13 from the cytosol to the membrane, since a constitutively membrane-attached, myristoylated Gα13 rescues spine morphology in the context of mutated palmitoylation sites (myr Gα13 CCSS; Fig. 8G). The different subcellular localization of the Gα13 variants was confirmed by cellular fractionation (Fig. 8H) and immunostaining (Suppl. Fig. 6A-C)

We conclude that miR-138 might inhibit spine growth, at least in part, by increasing membrane localization of Gα13 resulting in elevated activity of the downstream RhoA signaling pathway (Suppl. Fig. 6D).

Discussion

miRNAs have recently emerged as important regulators of vertebrate nervous system function, e.g. during neuronal differentiation (miR-9, miR-124), neuronal outgrowth (miR-132) and dendritic spine morphogenesis (miR-134) [23]. However, a systematic assessment of miRNA function, based on their temporal and subcellular expression in the brain, has not been achieved so far. In this study, we generated a comprehensive list of miRNAs that reside within the synaptodendritic compartment, and subsequently probed their function in the regulation of dendritic spine morphology. Thereby, we identified two neuronal miRNAs (miR-132, miR-138) that regulate dendritic spine size in an antagonistic manner. Two recent reports suggest that miRNAs beyond the ones identified here might participate in local translational control in dendrites [42, 43]. There is little overlap between these and our studies, which might be due to the different sample material (i.e. synaptosomes vs. cultured neurons, adult vs. P15 brain) and methodology (microarray vs. multiplex RT-PCR) used. However, we note that we might have missed low expressed miRNAs in dendrites due to our very stringent selection criteria. In addition, some of the miRNAs that we identified by microarray might have a function in dendrites that we were unable to uncover with our experimental setup. A more in-depth functional analysis of individual miRNAs identified here will improve our understanding of the dendritic miRNA network.

Based on multiple lines of evidence, APT1 is a bona fide miR-138 target mRNA in neurons. Studies in other cell systems document a role for APT1 in the depalmitoylation of a number of signaling proteins, including H-Ras, Gα subunits and endothelial nitric oxide synthase (eNOS). Although it was known that these APT1 substrates are important in synapse development, our results provide the first direct evidence for a biological function of APT1-dependent depalmitoylation in neurons during spine development. Using classical epistasis experiments, we found that Gα13 is one critical APT1 substrate in spine morphogenesis. Although monitoring Gα13 palmitoylation in neurons proved technically challenging, our results showing that miR-138 controls membrane localization of Gα13 in non-neuronal cells (Fig.8D, E) and that Gα13 palmitoylation is required for miR-138-dependent regulation of spine size (Fig. 8G) strongly suggest that miR-138 controls the level of Gα13 palmitoylation via APT1. Further work is needed to elucidate additional substrates of APT1 in neurons, and whether perturbation of miR-138 affects their palmitoylation. Obvious candidates besides Gα subunits include GPCRs, Fyn, Ras, eNOS and PSD-95, all of which are anchored to the spine membrane via palmitoylation [40]. Given that miRNAs usually regulate a large number of target mRNAs, miR-138 likely possesses physiologically relevant targets other than APT1. For example, EphrinB3 and RIMS2 contain canonical miR-138 seed matches in their 3'UTR, but none of them displayed a significant down-regulation upon miR-138 overexpression in neurons. The failure of these mRNAs to respond to miR-138 might be due to a low accessibility of the respective target sites in neurons (G.O., unpublished observation).

A major outcome of our study is that miRNA regulation in dendritic spines appears to converge on the translation of critical components of G-protein signaling pathways that impinge on the actin cytoskeleton (Suppl. Fig. 6D). For example, miR-134 inhibits expression of Limk1, a kinase that phosphorylates cofilin, an actin-binding protein which has been implicated in the regulation of dendritic spine and growth cone structure [44]. miR-132 has previously been shown to downregulate p250GAP, an important negative

regulator of the spine growth promoting GTPases Rac and Cdc42[32]. In this study we provide evidence that miR-138 mediates its effect on spine structure, at least in part, via regulation of the depalmitoylation enzyme APT1. Among the known APT1 substrates features Gα12/13, an activator of Rho downstream of G-protein coupled receptors [45]. A miR-138 mediated increase in Gα 12/13 palmitoylation and membrane localization could result in elevated Rho activity, which in turn could trigger spine shrinkage [46]. This novel miRNA-dependent layer of regulation of critical actin signaling components could help to adapt cytoskeletal changes in individual spines to changes in synaptic activity [6].

Our electrophysiological measurements demonstrate that miR-138 mediated spine shrinkage correlates with reduced postsynaptic function. Although the effects on mEPSC amplitudes are subtle, our results for the first time show a significant contribution of a neuronal miRNA to basal excitatory synaptic transmission. How miR-138 activity is regulated by stimuli that affect synapse morphology and function is an important topic for future studies. Our preliminary results indicate that, consistent with its spine growth inhibitory effect, miR-138 expression and activity are negatively regulated by calcium influx (Suppl. Fig. 3D, E). Whether activity-dependent regulation of miR-138 occurs at the level of precursor processing, as suggested by our previous results[47], or by a different mechanism remains to be determined. Nevertheless, it is an intriguing possibility that neuronal activity could regulate the expression and/or activity of a variety of synaptic miRNAs. This in turn could contribute to activity-dependent fine-tuning of signaling pathways that coordinate the structural and functional plasticity of spine synapses.

Materials and methods

Cell culture and transfection

Cultures of dissociated primary cortical and hippocampal neurons from embryonic day 18 (E18) Sprague Dawley rats (Charles River Laboratories, Sulzfeld, Germany) were prepared and cultured as described (Schratt et al., 2004). Neuronal transfections were performed with Lipofectamine 2000 (Invitrogen). For each well of a 24 well plate a total of 1μg DNA/RNA was mixed with a 1:50 dilution of Lipofectamine 2000 in Neurobasal Medium, incubated at room temperature for 20min and then further diluted 1:5 in Neurobasal Medium. Neurons were incubated with the transfection mix for 2h. Nucleofections were performed using the Rat Neuron Nucleofector Kit (Lonza) and program O-003. $4x10^6$ cells of rat primary cortical neurons (E18) were nucleofected with 2–3 μg total DNA per condition and plated on 6-well dishes in DMEM-Glutamax + 10% FBS (Invitrogen). After 5 h, medium was replaced with standard neuronal culture medium. Cholesterol-modified 2'O-me-oligonucleotides ("antagomirs", Thermo Scientific) were applied at 13DIV at 1 μM in conditioned culture medium for 24 h, and cells were lysed at 18 DIV.

HEK293 cells were maintained in DMEM (Invitrogen) plus 10% fetal bovine serum (Invitrogen), 1mM glutamine, 100 Units/ml penicillin and 100μg/ml streptomycin. Transfections were performed using the calcium phosphate method with a final calciumchloride concentration of 0.1M and an incubation time of 6–16h.

DNA constructs

The pSUPER RNAi expression system (Oligoengine) was used for siRNA-mediated knockdown of APT1 in cell culture. Four independent pSUPER constructs (APT1 shRNA 1 – 4) were generated using the Bgl*II* and Hind*III* restriction sites. pSuper plasmids were used either at 10 ng/ml (primary neurons) or 200 ng/ml (HEK293 cells). An expression vector for full-length mouse APT1 cDNA was obtained from OriGene (MC201121). A version with a mutated miR-138 binding site within the APT1 3'UTR (APT1 mutBS) was generated using

the QuikChange Site-Directed Mutagenesis Kit (Stratagene). For generation of an expression vector for myc-tagged $G_{\alpha}(13)$, the mouse $G_{\alpha}(13)$ ORF was PCR-amplified from the pCIS-$G_{\alpha}(13)$ expression vector (provided by S. Offermanns, Heidelberg) and then cloned into pcDNA™ 3.1/myc-His A (Invitrogen) using BamH*I* and Xba*I*. Refer to suppl. Methods for primer sequences.

Preparation of synaptoneurosomes

Synaptoneurosomes were prepared from P15 Sprague Dawley rat pups (Charles River, Sulzfeld, Germany) as described before [48]

Microarray

Please see the supplementary methods section for details.

Northern Blot

Northern blots to detect neuronal miRNAs and U6 snRNA were performed as described using radiolabeled DNA oligonucleotides as probes [19]

Western Blot

Proteins were separated by SDS-PAGE and blotted onto a PVDF membrane. Unspecific bindings were blocked with TBS plus 5% milk powder and 0,2% Tween20. The following primary antibodies were used: polyclonal rabbit anti-APT1 (1:1000; The anti-APT1 antibody was produced in rabbit from BioGenes (Berlin, Germany) using purified hAPT1 (provided by Robin Vetter, MPI für molekulare Physiologie, Dortmund, Germany)), mouse anti-PSD95 (1:1000; MA1-046, Dianova), mouse anti-cMyc (Santa Cruz, sc40), mouse anti-HA (Roche, 1583816), mouse anti-beta-3-tubulin (1:15000; MMS-435P, Covance), mouse anti-EEA1 (1:10000; 610456, Becton Dickinson), rabbit anti-Calnexin (SPA-865, Stressgen) and mouse anti-β-actin (A5441, Sigma). Primary antibodies were recognized either by an HRP-conjugated goat anti-rabbit antibody (1:20000; 401315, Calbiochem) or an HRP-conjugated rabbit anti-mouse antibody (1:20000; 402335, Calbiochem). Secondary antibodies were detected using the ECL Plus Western Blotting Detection System (GE Healthcare).

Image analysis

For image analysis, neurons were transfected at 10 DIV or 14 DIV with indicated miRNAs, miRNA-inhibitors or siRNA-expression vectors in combination with eGFP and processed for confocal microscopy at 18 DIV.

For spine analysis high-resolution z-stack images of GFP-positive neurons were taken with a confocal laser scanning microscope (Zeiss). Random neurons displaying pyramidal morphology were chosen from datasets that had been blinded to the experimental condition. Spine volumes were subsequently analyzed with the ImageJ software. At least 15 individual neurons derived from three independent experiments were measured for each experimental condition. For the functional screen 50 spines/neuron were analyzed, for subsequent analyses >100 spines/neuron. For Sholl analysis low magnification pictures of GFP-positive neurons were taken and dendritic complexity analyzed with the ImageJ software. At least ten individual neurons for each experimental condition of a total of three independent experiments were measured. For details on spine analysis and Sholl analysis see[19]. The determination of synapse density was performed according to 49. The size of GluR2 surface clusters was determined with the Analyze Particle function of ImageJ using thresholded images. Particles <0.1 μm^2 were excluded from the analysis.

Luciferase assay

Cortical or hippocampal neurons were transfected at 4 DIV or 14–16 DIV, and luciferase assays were performed 1 or 2 days later with the Dual-Luciferase Reporter Assay System (Promega).

In situ hybridization

In situ hybridization for APT1 was performed as described in [50] with a specific DIG-labeled RNA riboprobe (992 nts) sub-cloned into pBluescript II Sk(+) (Stratagene) vector for transcription.

For detection of endogenous miRNAs in dissociated neurons we basically followed the *in situ* hybridization protocol described in [48]. FITC-conjugated complementary locked nucleic acid (LNA) probes (Exiqon) were hybridized with miRNAs overnight at 50°C. The signal intensity of the FITC-probe was amplified using the Alexa Fluor® 488 Signal Amplification Kit (Molecular Probes). MAP2 immunostaining (mouse monoclonal, Sigma) was used to visualize dendrites.

Quantitative real-time PCR

Quantitative real-time PCR was performed with the 7300 Real Time PCR System (Applied Biosystems) using the iTaq SybrGreen Supermix with ROX (Bio-Rad) for detection of mRNAs and the specific TaqMan MicroRNA Assay kits (Applied Biosystems) for detection of small RNAs (PE Applied Biosystems).

Immunocytochemistry

Hippocampal neurons (17–18 DIV) were fixed in 4% paraformaldehyde for 15min, permeabilized with PBS plus 0,2% Triton X-100 and blocked in PBS plus 10% normal goat serum. We used a mouse monoclonal anti-PSD95 antibody (1:500; MA1-046, Dianova), a rabbit polyclonal anti-synapsin-1 antibody (1:500; Chemicon), a rabbit polyclonal anti-APT1 antibody (1:50; produced from BioGenes (Berlin, Germany)) or a HA-antibody (1:2000; Abcam ab9110) together with Cy3/Cy5-conjugated anti-mouse/rabbit antibodies (1:400, Jackson Immuno Research). GluR2 surface staining was performed as described [49].

Cell fractionation

Cells were scraped into ice-cold hypotonic buffer (5mM Tris, pH 7.5, 1mM $MgCl_2$, 1mM EGTA, 0,1mM EDTA) containing protease inhibitors (Complete Mini EDTA-free, Roche). Following 30min incubation on ice the lysate was passed through a 20-gauge needle 10 times and centrifuged at 3000×g for 15min to remove nuclear debris. The lysate was centrifuged again for 1h at 150000×g. The supernatant (cytosolic fraction) was collected and the pellet (membrane fraction) resuspendend in lysis buffer (50mM Tris pH 7.5, 150mM NaCl, 0,1% Triton-X-100, 0,2% SDS) containing protease inhibitors.

Application of APT1-inhibitors

Small molecule APT1-inhibitors (FD196, FD253, RB020) were diluted and stored in DMSO at a concentration of 10mM. Inhibitors were prediluted in medium and subsequently added to the cells with a final concentration of 10μM. The treatment was repeated every 60 min due to the high hydrolysis rate of the inhibitors. As control we added equivalent volumes of DMSO. A detailed characterization of the APT1 inhibitors will be published elsewhere.

Electrophysiology

Miniature excitatory postsynaptic currents (mEPSCs) were recorded in visually identified cultured neurons at DIV 18–20. Cover slips with transfected cells were constantly superfused with bath solution at RT (containing in mM: NaCl 156, KCl 2, $CaCl_2$ 2, $MgCl_2$ 1, glucose 16.5, HEPES 10; pH 7.3, 330 mOsmol). Pipette solution for whole cell recording contained (in mM) KCl 100, NaCl 10, $CaCl_2$ 0.25, EGTA 5, HEPES 10, glucose 40, Mg-ATP 4, Na-GTP 0.1; pH set at 7.3, 310 mOsmol. During recording, the bath solution contained gabazine (5 μM) and tetrodotoxin (0.5 μM). See Suppl. Material fur further details.

Supplementary Material

Refer to Web version on PubMed Central for supplementary material.

Acknowledgments

We thank O. Rocks, S. Offermanns, R. Vetter and P. Wedegaertner for generously providing reagents and R. Heinen on suggestions for the luciferase reporter assays. The excellent technical assistance by T. Wüst is greatly acknowledged. M. Alenius and A. Keene critically read the manuscript. This work was supported by the Deutsche Forschungsgemeinschaft (SFB488; G.M.S.), the Human Frontier Science Program (Career Development Award; G.M.S.), the National Institute on Drug Abuse (1R21DA025102-01; G.M.S.), the NIH (NS045500; M.E.G.) the Bioinformatics Initiative (C. D. and M. R.), the Austrian Academy of Sciences (J.M. and S.B. (DOC-fFORTE-fellowship)) and the Austrian Government, GEN-AU initiative (G.O.).

References

1. Hering H, Sheng M. Dendritic spines: structure, dynamics and regulation. Nat Rev Neurosci. 2001; 2:880–888. [PubMed: 11733795]
2. Nimchinsky EA, Sabatini BL, Svoboda K. Structure and function of dendritic spines. Annu Rev Physiol. 2002; 64:313–353. [PubMed: 11826272]
3. Matsuzaki M, Honkura N, Ellis-Davies GC, Kasai H. Structural basis of long-term potentiation in single dendritic spines. Nature. 2004; 429:761–766. [PubMed: 15190253]
4. Nagerl UV, Eberhorn N, Cambridge SB, Bonhoeffer T. Bidirectional activity-dependent morphological plasticity in hippocampal neurons. Neuron. 2004; 44:759–767. [PubMed: 15572108]
5. Bagni C, Greenough WT. From mRNP trafficking to spine dysmorphogenesis: the roots of fragile X syndrome. Nat Rev Neurosci. 2005; 6:376–387. [PubMed: 15861180]
6. Okamoto K, Nagai T, Miyawaki A, Hayashi Y. Rapid and persistent modulation of actin dynamics regulates postsynaptic reorganization underlying bidirectional plasticity. Nat Neurosci. 2004; 7:1104–1112. [PubMed: 15361876]
7. Yi JJ, Ehlers MD. Ubiquitin and protein turnover in synapse function. Neuron. 2005; 47:629–632. [PubMed: 16129392]
8. Shi SH, et al. Rapid spine delivery and redistribution of AMPA receptors after synaptic NMDA receptor activation. Science. 1999; 284:1811–1816. [see comments.]. [PubMed: 10364548]
9. Zhou Z, et al. Brain-Specific Phosphorylation of MeCP2 Regulates Activity- Dependent Bdnf Transcription, Dendritic Growth, and Spine Maturation. Neuron. 2006; 52:255–269. [PubMed: 17046689]
10. Bingol B, Schuman EM. Synaptic protein degradation by the ubiquitin proteasome system. Curr Opin Neurobiol. 2005; 15:536–541. [PubMed: 16150592]
11. Steward O, Schuman EM. Protein synthesis at synaptic sites on dendrites. Annual Review of Neuroscience. 2001; 24:299–325.
12. Martin KC, Barad M, Kandel ER. Local protein synthesis and its role in synapse-specific plasticity. Curr Opin Neurobiol. 2000; 10:587–592. [PubMed: 11084321]

13. Eberwine J, Miyashiro K, Kacharmina JE, Job C. Local translation of classes of mRNAs that are targeted to neuronal dendrites. Proceedings of the National Academy of Sciences of the United States of America. 2001; 98:7080–7085. [PubMed: 11416191]
14. Ostroff LE, Fiala JC, Allwardt B, Harris KM. Polyribosomes redistribute from dendritic shafts into spines with enlarged synapses during LTP in developing rat hippocampal slices. Neuron. 2002; 35:535–545. [PubMed: 12165474]
15. Wells DG, Richter JD, Fallon JR. Molecular mechanisms for activityregulated protein synthesis in the synapto-dendritic compartment. Current Opinion in Neurobiology. 2000; 10:132–137. [PubMed: 10679431]
16. Kiebler MA, Bassell GJ. Neuronal RNA granules: movers and makers. Neuron. 2006; 51:685–690. [PubMed: 16982415]
17. Krichevsky AM, Kosik KS. Neuronal RNA granules: a link between RNA localization and stimulation-dependent translation. Neuron. 2001; 32:683–696. [PubMed: 11719208]
18. Ashraf SI, McLoon AL, Sclarsic SM, Kunes S. Synaptic protein synthesis associated with memory is regulated by the RISC pathway in Drosophila. Cell. 2006; 124:191–205. [PubMed: 16413491]
19. Schratt GM, et al. A brain-specific microRNA regulates dendritic spine development. Nature. 2006; 439:283–289. [PubMed: 16421561]
20. Ambros V. The functions of animal microRNAs. Nature. 2004; 431:350–355. [PubMed: 15372042]
21. Bartel DP. MicroRNAs: genomics, biogenesis, mechanism, and function. Cell. 2004; 116:281–297. [PubMed: 14744438]
22. Filipowicz W, Bhattacharyya SN, Sonenberg N. Mechanisms of posttranscriptional regulation by microRNAs: are the answers in sight? Nat Rev Genet. 2008; 9:102–114. [PubMed: 18197166]
23. Kosik KS. The neuronal microRNA system. Nat Rev Neurosci. 2006; 7:911–920. [PubMed: 17115073]
24. Miska EA, et al. Microarray analysis of microRNA expression in the developing mammalian brain. Genome Biol. 2004; 5:R68. [PubMed: 15345052]
25. Sempere LF, et al. Expression profiling of mammalian microRNAs uncovers a subset of brain-expressed microRNAs with possible roles in murine and human neuronal differentiation. Genome Biol. 2004; 5:R13. [PubMed: 15003116]
26. Kim J, et al. Identification of many microRNAs that copurify with polyribosomes in mammalian neurons. Proc Natl Acad Sci U S A. 2004; 101:360–365. [PubMed: 14691248]
27. Yeh DC, Duncan JA, Yamashita S, Michel T. Depalmitoylation of endothelial nitric-oxide synthase by acyl-protein thioesterase 1 is potentiated by Ca(2+)-calmodulin. J Biol Chem. 1999; 274:33148–33154. [PubMed: 10551886]
28. Rao A, Steward O. Evidence that protein constituents of postsynaptic membrane specializations are locally synthesized: analysis of proteins synthesized within synaptosomes. J Neurosci. 1991; 11:2881–2895. [PubMed: 1880554]
29. Meister G, Landthaler M, Dorsett Y, Tuschl T. Sequence-specific inhibition of microRNA- and siRNA-induced RNA silencing. Rna. 2004; 10:544–550. [PubMed: 14970398]
30. Zito K, Knott G, Shepherd GM, Shenolikar S, Svoboda K. Induction of spine growth and synapse formation by regulation of the spine actin cytoskeleton. Neuron. 2004; 44:321–334. [PubMed: 15473970]
31. Mansfield JH, et al. MicroRNA-responsive 'sensor' transgenes uncover Hoxlike and other developmentally regulated patterns of vertebrate microRNA expression. Nat Genet. 2004; 36:1079–1083. [PubMed: 15361871]
32. Vo N, et al. A cAMP-response element binding protein-induced microRNA regulates neuronal morphogenesis. Proc Natl Acad Sci U S A. 2005; 102:16426–16431. [PubMed: 16260724]
33. Rehmsmeier M, Steffen P, Hochsmann M, Giegerich R. Fast and effective prediction of microRNA/target duplexes. Rna. 2004; 10:1507–1517. [PubMed: 15383676]
34. Kruger J, Rehmsmeier M. RNAhybrid: microRNA target prediction easy, fast and flexible. Nucleic Acids Res. 2006; 34:W451–W454. [PubMed: 16845047]

35. Rodenas-Ruano A, Perez-Pinzon MA, Green EJ, Henkemeyer M, Liebl DJ. Distinct roles for ephrinB3 in the formation and function of hippocampal synapses. Dev Biol. 2006; 292:34–45. [PubMed: 16466709]
36. Etournay R, et al. PHR1, an integral membrane protein of the inner ear sensory cells, directly interacts with myosin 1c and myosin VIIa. Journal of cell science. 2005; 118:2891–2899. [PubMed: 15976448]
37. Ozaki N, et al. cAMP-GEFII is a direct target of cAMP in regulated exocytosis. Nat Cell Biol. 2000; 2:805–811. [PubMed: 11056535]
38. El-Husseini Ael D, et al. Synaptic strength regulated by palmitate cycling on PSD-95. Cell. 2002; 108:849–863. [PubMed: 11955437]
39. Linder ME, Deschenes RJ. Palmitoylation: policing protein stability and traffic. Nature reviews. 2007; 8:74–84.
40. Kang R, et al. Neural palmitoyl-proteomics reveals dynamic synaptic palmitoylation. Nature. 2008; 456:904–909. [PubMed: 19092927]
41. Bhattacharyya R, Wedegaertner PB. Galpha 13 requires palmitoylation for plasma membrane localization, Rho-dependent signaling, and promotion of p115-RhoGEF membrane binding. J Biol Chem. 2000; 275:14992–14999. [PubMed: 10747909]
42. Kye MJ, et al. Somatodendritic microRNAs identified by laser capture and multiplex RT-PCR. Rna. 2007
43. Lugli G, Torvik VI, Larson J, Smalheiser NR. Expression of microRNAs and their precursors in synaptic fractions of adult mouse forebrain. J Neurochem. 2008
44. Bernard O. Lim kinases, regulators of actin dynamics. The international journal of biochemistry & cell biology. 2007; 39:1071–1076.
45. Kurose H. Galpha12 and Galpha13 as key regulatory mediator in signal transduction. Life sciences. 2003; 74:155–161. [PubMed: 14607242]
46. Tada T, Sheng M. Molecular mechanisms of dendritic spine morphogenesis. Curr Opin Neurobiol. 2006; 16:95–101. [PubMed: 16361095]
47. Obernosterer G, Leuschner PJ, Alenius M, Martinez J. Posttranscriptional regulation of microRNA expression. RNA. 2006; 12:1161–1167. [PubMed: 16738409]
48. Schratt GM, Nigh EA, Chen WG, Hu L, Greenberg ME. BDNF regulates the translation of a select group of mRNAs by a mammalian target of rapamycin-phosphatidylinositol 3-kinase-dependent pathway during neuronal development. J Neurosci. 2004; 24:9366–9377.
49. Paradis S, et al. An RNAi-Based Approach Identifies Molecules Required for Glutamatergic and GABAergic Synapse Development. Neuron. 2007; 53:217–232. [PubMed: 17224404]
50. Obernosterer G, Martinez J, Alenius M. Locked nucleic acid-based in situ detection of microRNAs in mouse tissue sections. Nat Protoc. 2007; 2:1508–1514. [PubMed: 17571058]

A

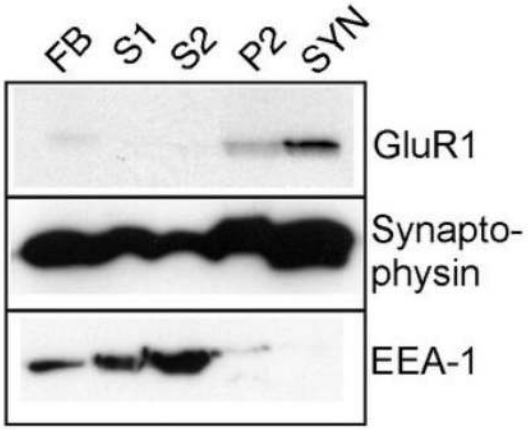

B

miRNA	Fold enrichment	STDV
miR-29a	4,60	2,45
miR-7	3,71	1,65
miR-341	3,41	1,09
miR-218	3,39	1,17
miR-137	3,27	0,61
miR-9	2,66	1,39
miR-335	2,25	0,45
miR-376b	2,20*	0,44
miR-98	2,19*	0,51
miR-138	2,16	0,51
miR-143	0,36	0,07
miR-150	0,25	0,10
miR-145	0,20	0,06
miR-126	0,05	0,01

C

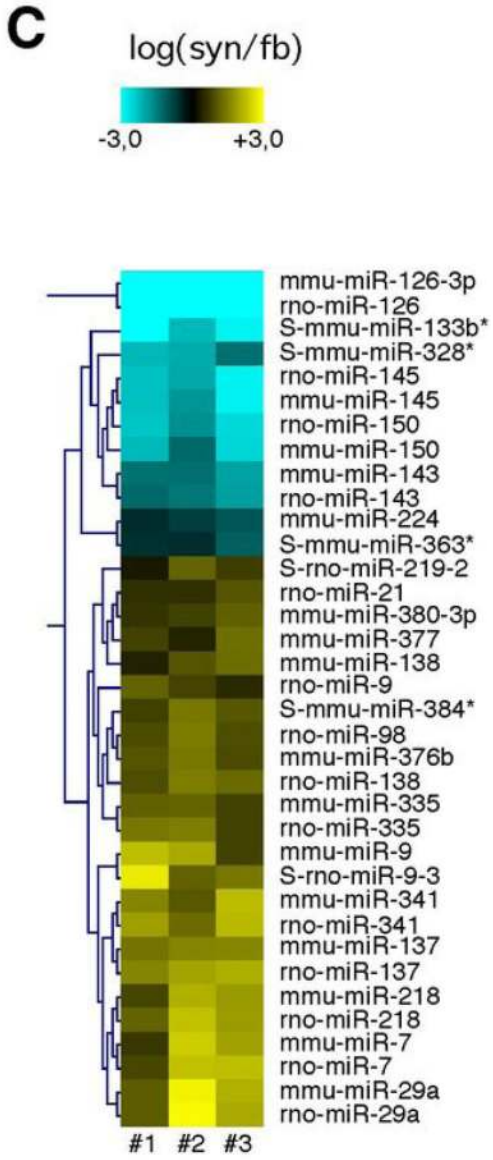

Figure 1. Expression profiling of miRNAs in synaptososomes

A) Western blot analysis of protein extracts derived from P15 rat forebrain (FB), low-speed centrifugation supernatant (S1), high-speed centrifugation supernatant (S2), high-speed centrifugation pellet (membrane, P2) or synaptosomes (SYN). Whereas pre- (synaptophysin) and postsynaptic proteins (GluR1) are enriched in SYN, the cytoplasmic EEA-1 is depleted from P2 and SYN.

B) List of miRNAs that displayed an at least twofold change in expression between synaptosomes and forebrain in three different experiments.

C) Hierarchical clustering of miRNAs displaying significantly different expression between whole forebrain and synaptosomes in three different experiments. Colour coding: enrichment in synaptosomes (syn) vs. whole forebrain (fb) in logarithmic scale, yellow=enriched in synaptosomes, blue=depleted in synaptosomes.

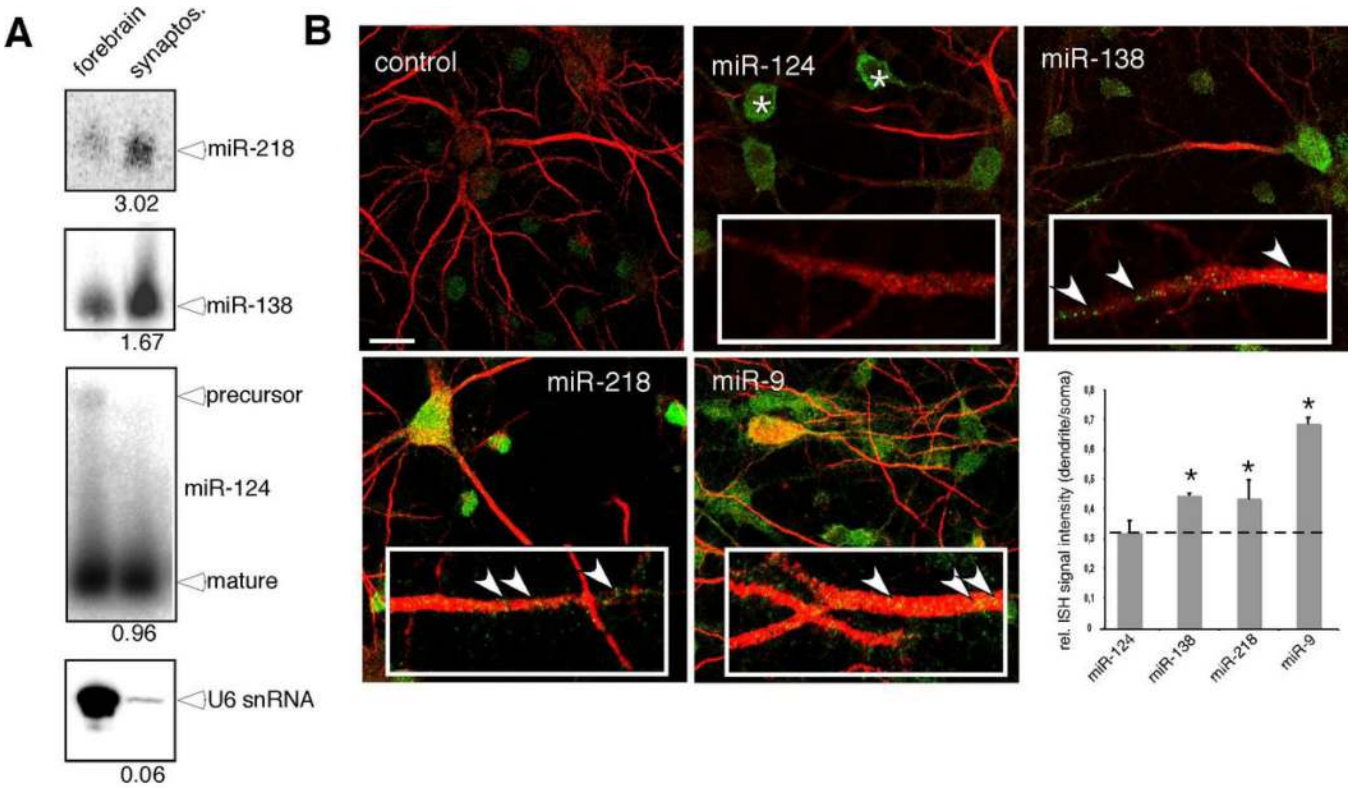

Figure 2. A subset of neuronal miRNAs is localized in the synaptodendritic compartment

A) Validation of microarray results by Northern blot. RNA was extracted from P15 rat forebrain or P15 rat synaptosomes, separated on 15% PAGE and probed for the presence of miR-218, miR-138, miR-124 or U6 snRNA. Numbers represent fold enrichment in synaptosomes. Note the absence of premiR-124 from synaptosomes.

B) Subcellular localization of synaptically enriched miRNAs in hippocampal neurons. *In situ* hybridization was performed on hippocampal neurons at 18 DIV using FITC-coupled LNA probes directed against miR-9, miR-218 and miR-124, a DIG-coupled LNA probe directed against miR-138 or a DIG-coupled control LNA probe. Asterisks: Prominent staining of miR-124 in neuronal cell bodies. Arrowheads: Dendritic staining of miR-134, miR-218 and miR-138. Scale bar = 20 μm. Lower right panel: Quantification of ISH signal. Values are expressed as ratio between dendritic and somatic signal intensities. Dendrite/soma ratios of miR-138, miR-218 and miR-9 are significantly higher than the ratio of the somatic miR-124. * $p<0.05$ (t-test, n=3).

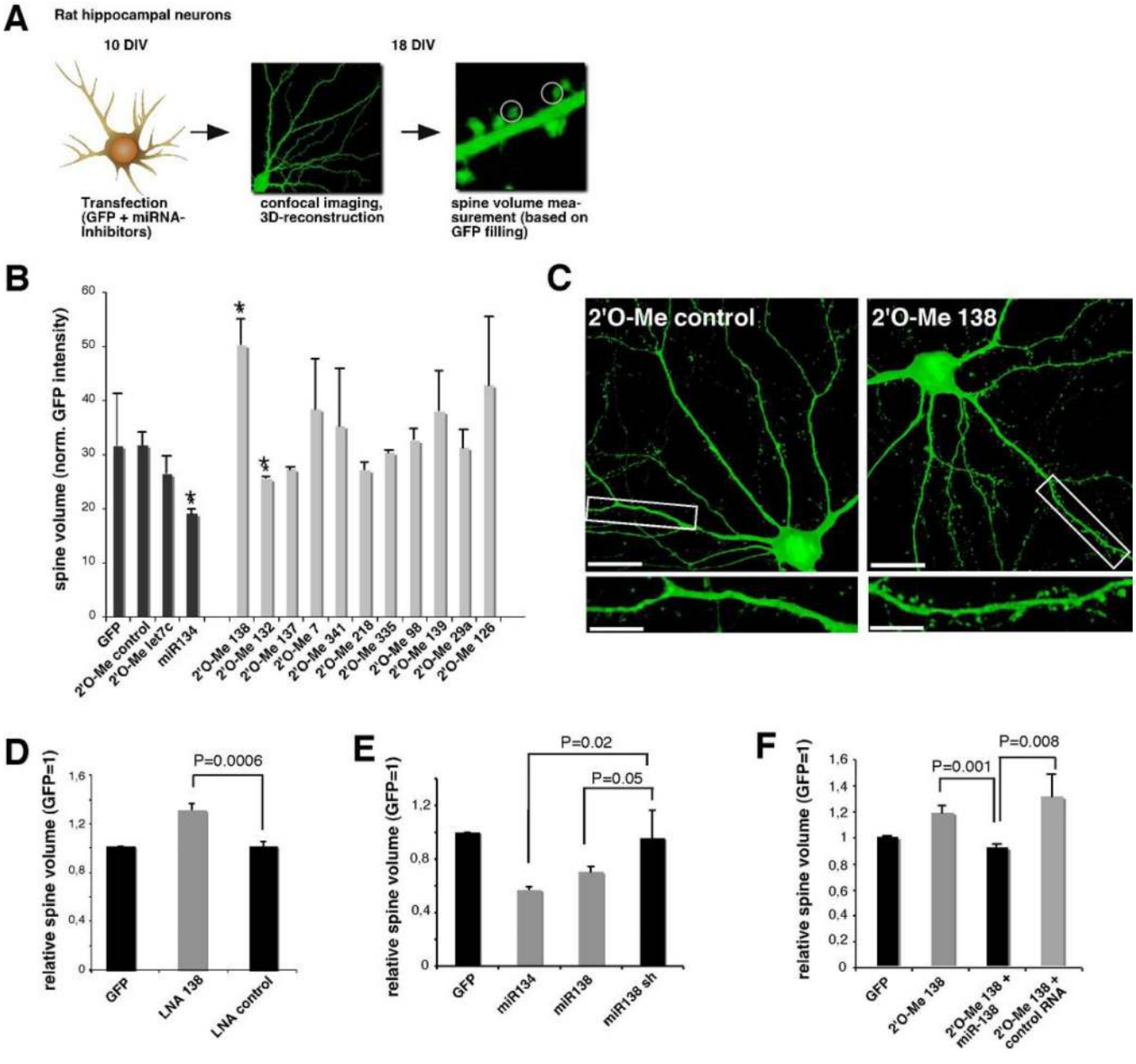

Figure 3. The synaptically enriched miR-138 regulates dendritic spine size

A) Flowchart of the functional screen for the identification of miRNAs controlling dendritic spine size. Rat hippocampal neurons (10 DIV) were transfected with GFP together with miRNA inhibitors (40 nM) or 134 duplex RNA (20 nM), and processed at 18 DIV for confocal microscopy. Fluorescence intensity of the freely diffusible GFP within 3D projections was used to calculate relative spine volume.

B) Quantitative analysis of relative spine volume of hippocampal neurons transfected with the indicated double-stranded (ds) RNA (20 nM) or antisense 2'-O-methyl (2'O-me) oligonucleotides (40 nM). Values represent the mean ± S.D. (n=3; at least 750 spines from 15 neurons). *p<0.05 (compared to 2'O-methyl control conditions).

C) Representative hippocampal neurons (18 DIV) transfected with GFP together with either 2'O-me control (left panel) or 2'O-me 138 (40 nM). Boxed insets display spines at higher magnification. Scale bars: 20 μm (overview); 8 μm (inset).

D) LNA-mediated inhibition of miR-138 increases spine volume. Average spine volume of neurons treated with the indicated LNA antisense oligonucleotides (100 nM). Values were normalized to the GFP-only condition and represent the mean ± S.D. (n=3; at least 1200 spines from 15 neurons). p=0.001 (ANOVA). P-value of pairwise Student`s t-test is indicated.

E) Overexpression of miR-138 in hippocampal neurons reduces spine volume. Duplex RNAs representing the full-length version of miR-138, a 3' truncated miR-138 (miR138 sh) or miR-134 were transfected as in B and relative spine volume was determined. Values were normalized to the GFP-only condition and represent the mean ± S.D. (n=3; at least 1200 spines from 15 neurons). P=0.029 (ANOVA). P-values of pairwise Student's t-tests are indicated.

F) Restoring miR-138 function rescues increased spine size caused by miR-138 inhibition. Average spine volume was determined from neurons transfected with 2'O-me-138 (40 nM) together with synthetic miR-138 duplex RNA (20 nM) or control duplex RNA (20 nM, let-7c). Values were normalized to the GFP-only condition and represent the mean ± S.D. (n=3; at least 1200 spines from 15 neurons). P=0.0067 (ANOVA). P-values of pairwise Student's t-tests are indicated.

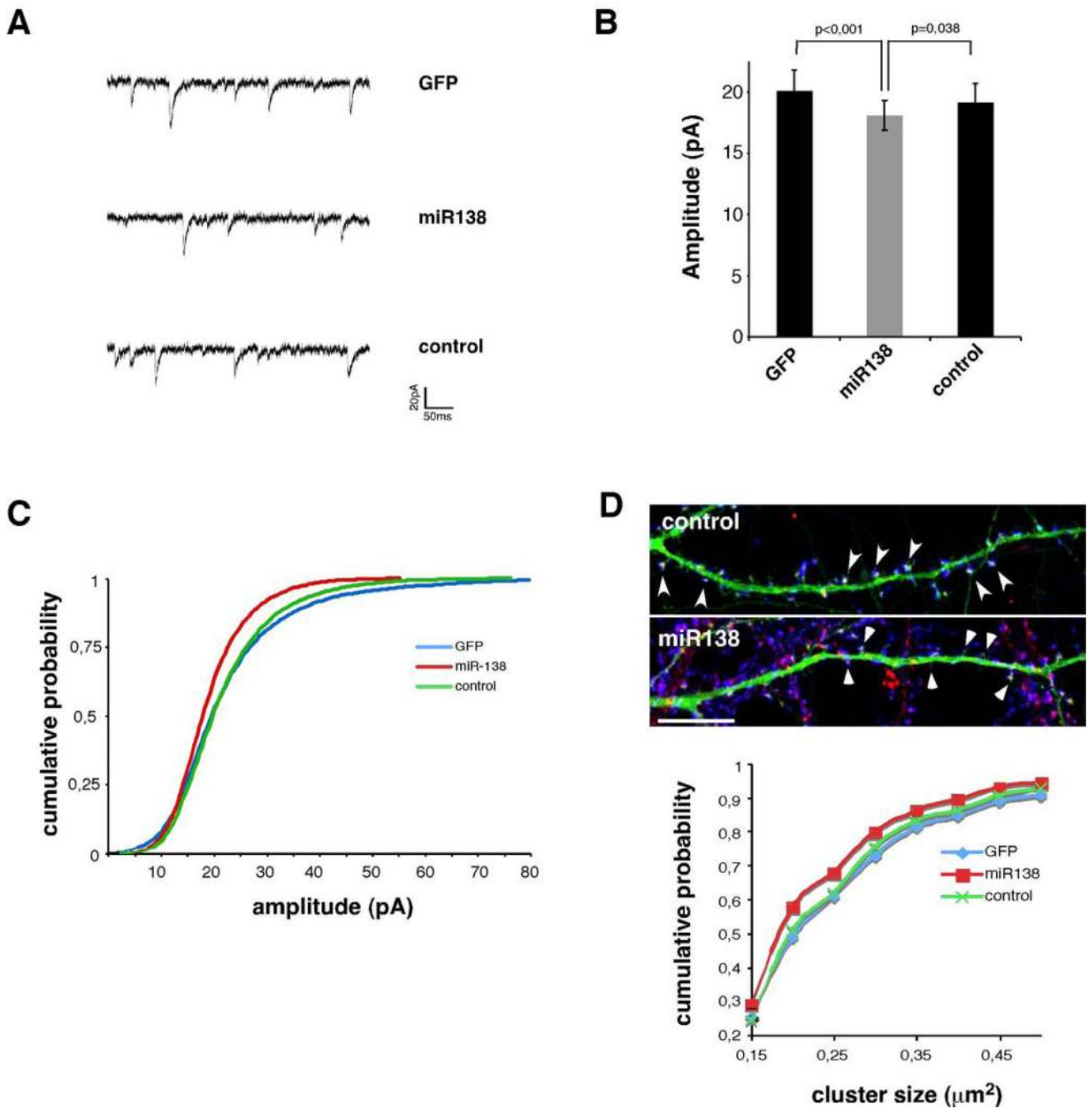

Figure 4. miR-138 negatively regulates miniature synaptic transmission at excitatory synapses

A) Original recordings of mEPSCs in cultured hippocampal neurons in the presence of TTX and gabazine. Cells were voltage clamped at −70 mV. Traces show representative data from cells expressing GFP only, GFP + miR-138 duplex RNA, and control duplex RNA, respectively.

B) Reduction of median mEPSC amplitudes in miR138 expressing neurons. Bars show the mean value and standard deviation of medians for each group (GFP n = 14; miR-138 n = 16; control duplex RNA n = 12). p-values (pairwise Student's t-test) are indicated above bar graph.

C) Cumulative amplitude distributions of mEPSCs recorded from neurons transfected as in A). Data pooled from 14 cells (GFP), 16 cells (mir-138), and 12 cells (control duplex RNA). Note leftward shift of cumulative curve for miR-138 ($p < 0.001$, Kolmogorov-Smirnov test). D) GluR2 surface staining of cells transfected as in A). Upper panel: Representative dendrites of neurons transfected with either miR-138 or control duplex RNA and stained for GluR2 (red) and synapsin (blue). Arrowheads depict large GluR2 clusters in spine heads of control neurons and small or absent GluR2 clusters in protrusions of miR-138 expressing neurons. Scale bar: 10 μm. Lower panel: The cumulative distribution of GluR2 surface cluster sizes is plotted for the indicated conditions. KS-test: p=0.001; D: 0,0927 (miR-138 vs. control transfected cells).

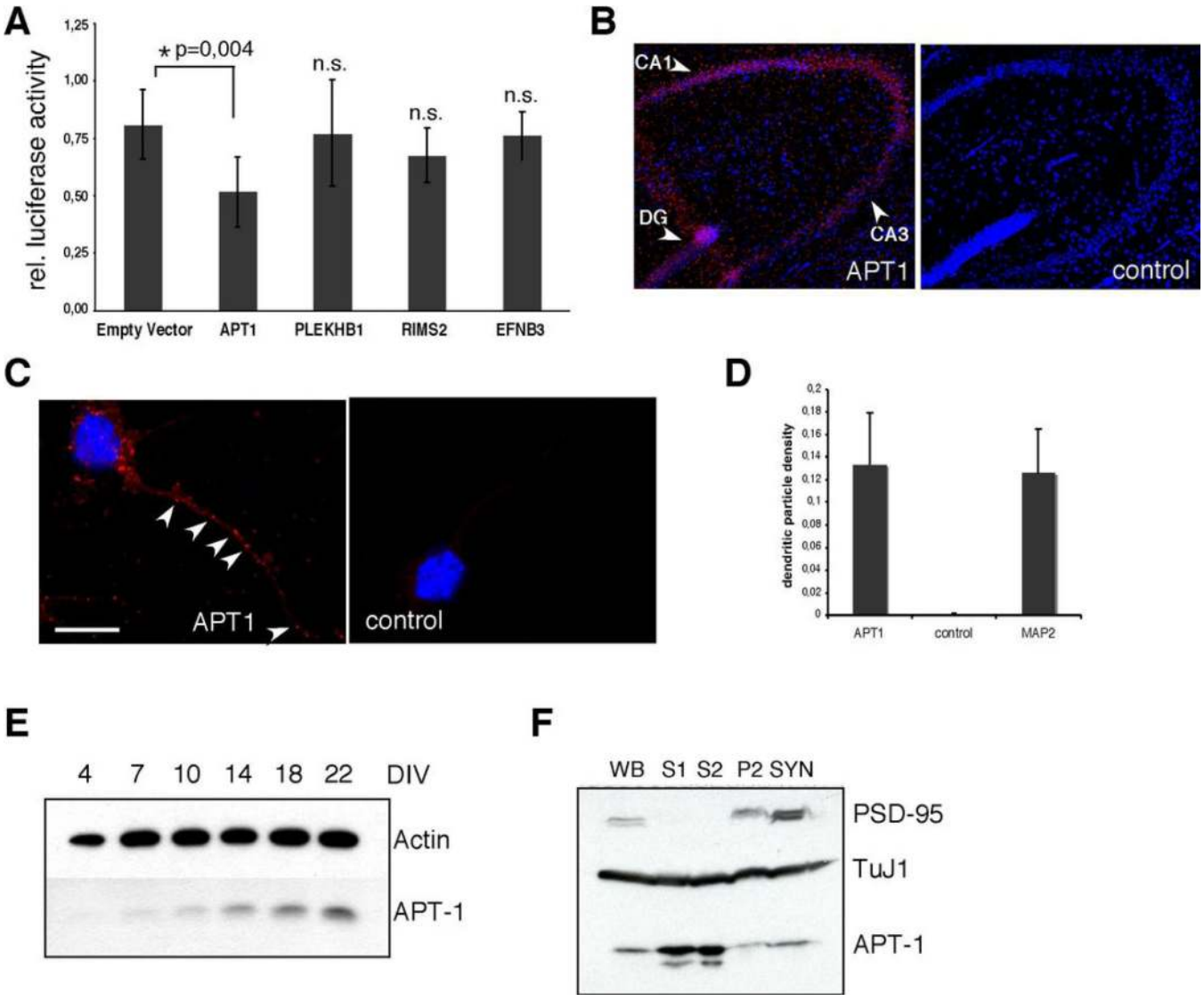

Figure 5. APT1 is expressed in neuronal dendrites during synapse development

A) Validation of predicted miR-138 target mRNAs by dual-luciferase reporter assay in cortical neurons (5 DIV). 3'UTR regions of the indicated genes were cloned downstream of the firefly luciferase coding region within pGL3, and the resulting vectors were transfected into neurons together with miR-138 duplex RNA (20 nM). Percent firefly luciferase activity, normalized to the internal Renilla luciferase control, of miR-138 expressing cells compared to control-transfected cells is plotted for each individual reporter construct. Error bars represent the mean ± S.D. (empty vector: n=5; APT1: n=6), each performed in duplicate. * $p<0.05$ (pairwise Student's t-test; individual pvalues are indicated above each bar)

B) APT1 mRNA is expressed in mouse hippocampus. *In situ* hybridization (ISH) was performed in adult mouse hippocampal slices using a probe perfectly complementary to mouse APT1 mRNA (red signal, left panel) or a mismatch control probe (right panel). Cell nuclei were visualized by Hoechst counterstain (blue signal). DG: dentate gyrus.

C) APT1 mRNA localizes to dendrites of primary hippocampal neurons. ISH was performed in 9–10 DIV primary dissociated hippocampal neurons as described in B. Note the presence of multiple dendritic APT1 mRNA-containing granules along the entire length of dendrites (arrowheads). Scale bar: 20 μm.

D) Quantification of ISH signals obtained in C. Data represent the mean ± S.D. for each of the indicated ISH probes (n=6 (APT1, control); n=8 (MAP2)).
E) APT1 protein expression is upregulated during the development of primary cortical neurons in culture. Whole cell extracts were prepared from the indicated stages of cortical neuron development and simultaneously probed with a rabbit antiserum against APT1 (lower band) and a mouse monoclonal anti-β-Actin antibody as a loading control (upper band).
F) APT1 protein is present at low levels in synaptosomal extracts. P15 rat brains were fractionated into cytosolic fractions (S1, S2), membranous fraction (P2) and synaptosomes (SYN), and fractions were probed for the presence of PSD-95, APT1 and TuJ1 as a loading control. Protein levels in whole forebrain before fractionation (WB) are shown for comparison.

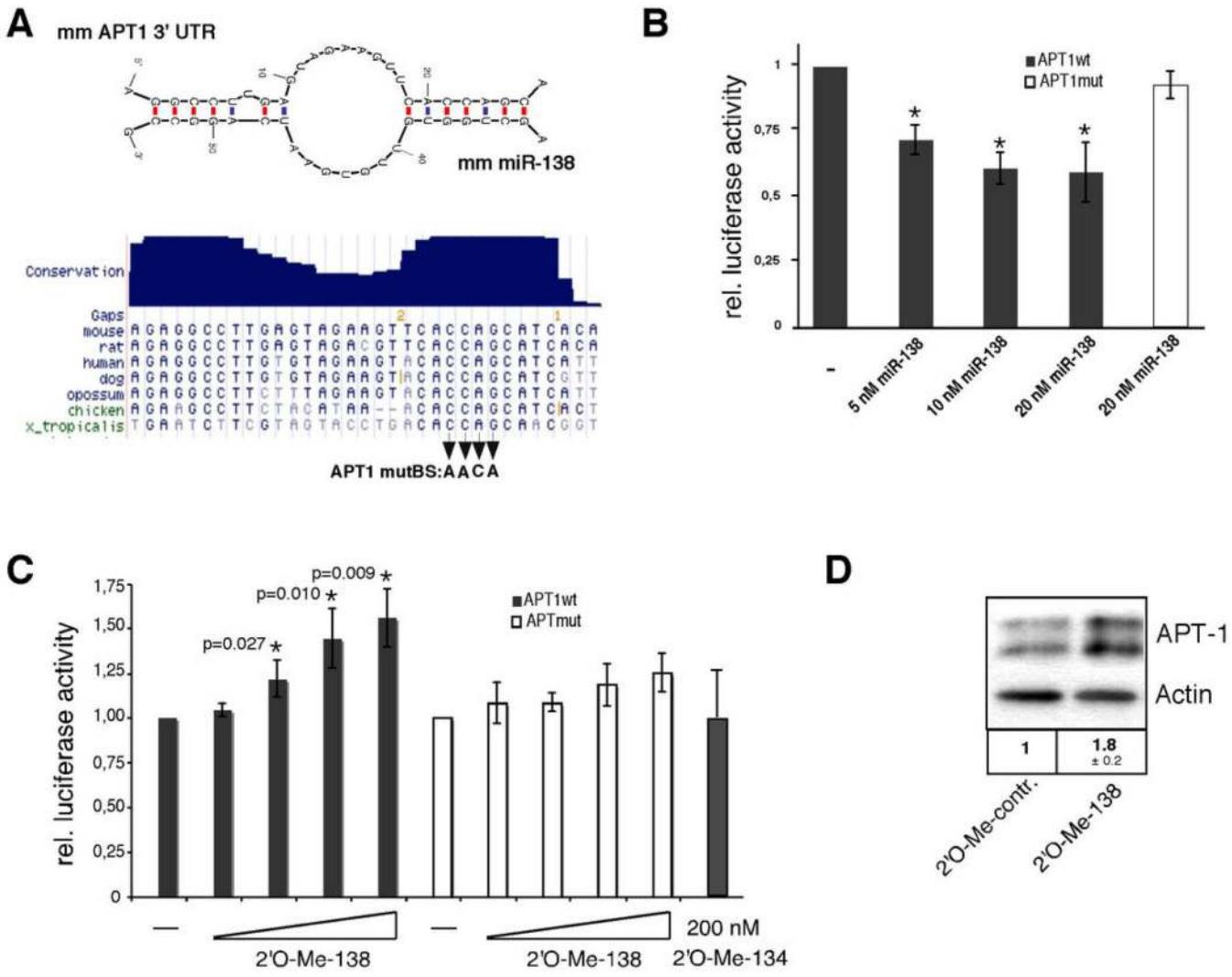

Figure 6. APT1 is a miR-138 target mRNA in neurons

A) Schematic representation of the mouse miR-138-APT1 3'UTR duplex as determined by RNAfold. G:C base pairs are indicated by red, A:U and G:U base pairs by blue dots. Lower panel: Sequence conservation of the miR-138 target site within the APT1 3'UTR across the indicated vertebrate species. Note the extensive conservation of nucleotides at both ends of the duplex that are engaged in base-pairing, and the less extensive conservation in the internal bulge structure (adopted from UCSC genome browser). Nucleotide substitutions in the APT1 mutBS construct are indicated.

B) Importance of the "seed" region within the APT1 3'UTR for miR-138 mediated downregulation in primary rat cortical neurons (5 DIV). Luciferase assay was performed with APT1 wt and mut 3'UTR constructs in the presence of the indicated concentrations of miR-138 duplex RNA. Values are expressed relative to the internal Renilla luciferase activity and normalized to the activity of the APT1 wt reporter under basal conditions. Bars represent the mean ± S.D. (10 nM: n=6; 20 nM: n=18; APT1 mut: n=8). *p<0.00001 (pairwise Student's t-test between corresponding values of wt and mut reporter).

C) Endogenous miR-138 inhibits APT1 luciferase reporter gene expression. APT1 wt or mut luciferase reporter genes were co-transfected together with increasing amounts of 2'O-me-138 AS oligonucleotide (50–200 nM) into hippocampal neurons (16 DIV) and luciferase activity was measured two days later. Results represent the mean ± S.D. (n=5). Activity of

the APT1 wt and mut reporters under basal conditions was arbitrarily set to one. *$p<0.01$ (pairwise Student's t-test between corresponding values of wt and mut reporter; p-values are shown above bar graphs).

D) Endogenous miR-138 inhibits accumulation of APT1 protein. Cholesterol-modified 2'O-methyl antisense oligonucleotides directed against miR-138 or an unrelated sequence (scrambled) were introduced into hippocampal neurons at 13 DIV at a concentration of 1 μM, and protein extracts were prepared for Western blotting at 18 DIV. The average fold increase of the APT1 signal is indicated (n=3; 2'O-me control = 1).

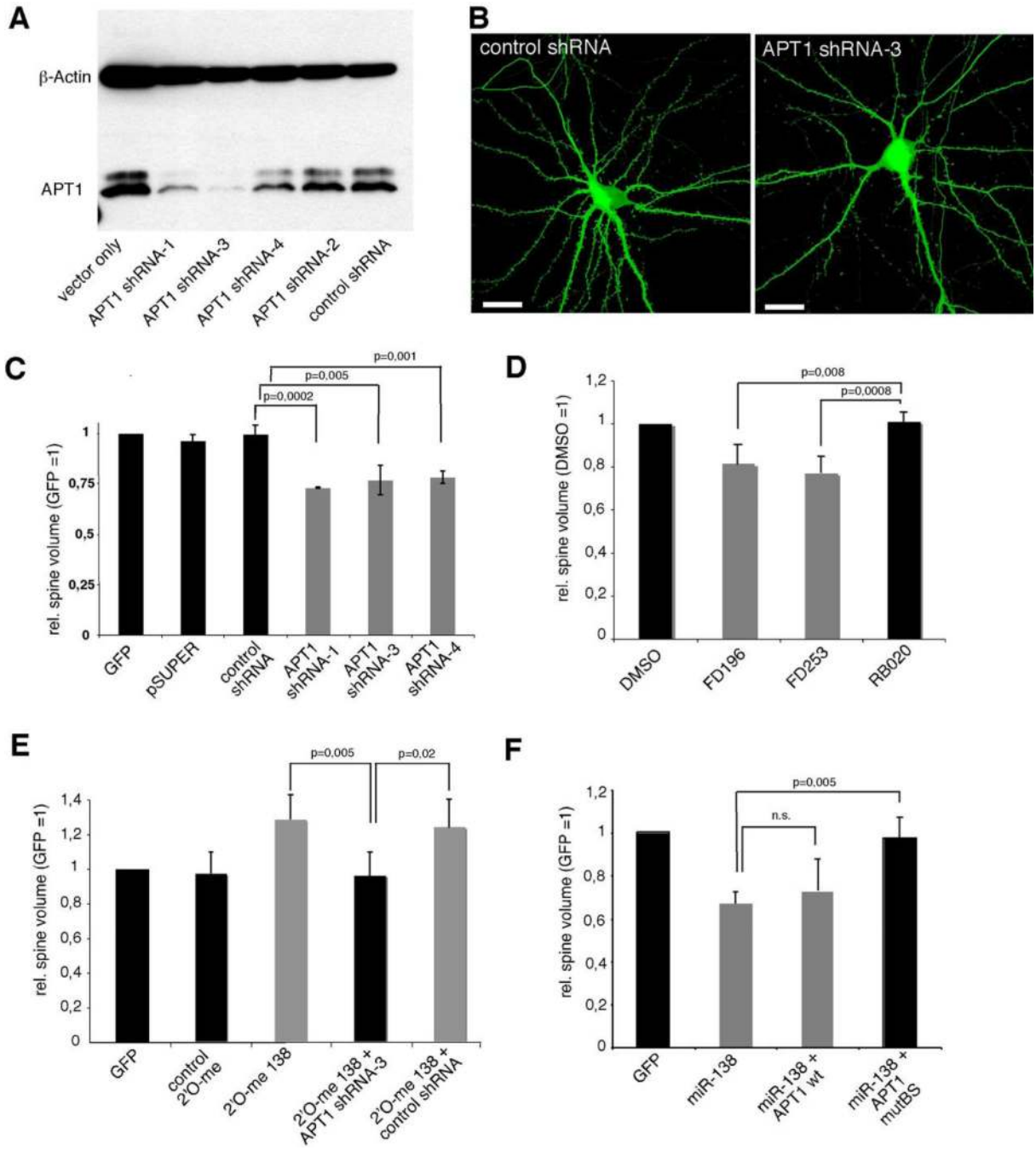

Figure 7. APT1 activity is required for the control of dendritic spine size

A) shRNA-mediated knockdown of endogenous APT1 in primary neurons. 2 μg of pSuper shRNA vectors were electroporated into cortical neurons, and expression of endogenous APT1 and β-Actin were determined by Western blotting (7DIV).

B) Interfering with APT1 expression in neurons reduces dendritic spine volume. Representative hippocampal neurons at 18 DIV transfected with eGFP and either control shRNA (left panel) or pSuper-APT1-shRNA-3 are shown. Scale bar = 20 μm.

C) shRNA-mediated knockdown of endogenous APT1 in neurons reduces dendritic spine volume. Rat hippocampal neurons (14 DIV) were transfected with GFP alone or together with pSuper expressing shRNAs directed against APT1 mRNA (APT1 shRNA-1, 3 and 4)

or an unrelated sequence (control shRNA, 5 ng/ml each). Values were normalized to the GFP-only condition and represent the mean ± S.D. (n=3; at least 1800 spines from 18 neurons). p<0.0001 (ANOVA). P-values of pairwise student's t-tests are indicated.
D) Pharmacological inhibition of APT1 in neurons reduces dendritic spine volume. Hippocampal neurons (18 DIV) were treated for 6 h with either inactive control compound (RB020) or specific APT1 inhibitors (FD196, FD253, 10 μM each) before analyzing spine volume. Values were normalized to the DMSO-only condition and represent the mean ± S.D. (n=3; 1800 spines from 18 neurons). p=0.044 (ANOVA). P-values of pairwise Student's t-tests are indicated.
E) shRNA-mediated knockdown of APT1 suppresses the increase in spine volume caused by miR-138 inhibition. Rat hippocampal neurons (14 DIV) were transfected with the indicated 2'O-me antisense oligonucleotides (40 nM) together with APT1 shRNA-3 or control shRNA (5 ng each). Values represent the mean ± S.D. (n=4; at least 2400 spines of 24 neurons). p=0.0075 (ANOVA). P-values of pairwise Student's t-tests are indicated.
F) APT1 expression rescues miR-138 mediated spine shrinkage. Rat hippocampal neurons (10 DIV) were transfected with miR-138 duplex RNA (20 nM) in combination with APT1 wt or APT1 mutBS (250ng/ml each). Values were normalized to the GFP-only condition and represent the mean ± S.D. (n=3; at least 1800 spines from 18 neurons). p=0.029 (ANOVA). P-values of pairwise Student's t-tests are indicated.

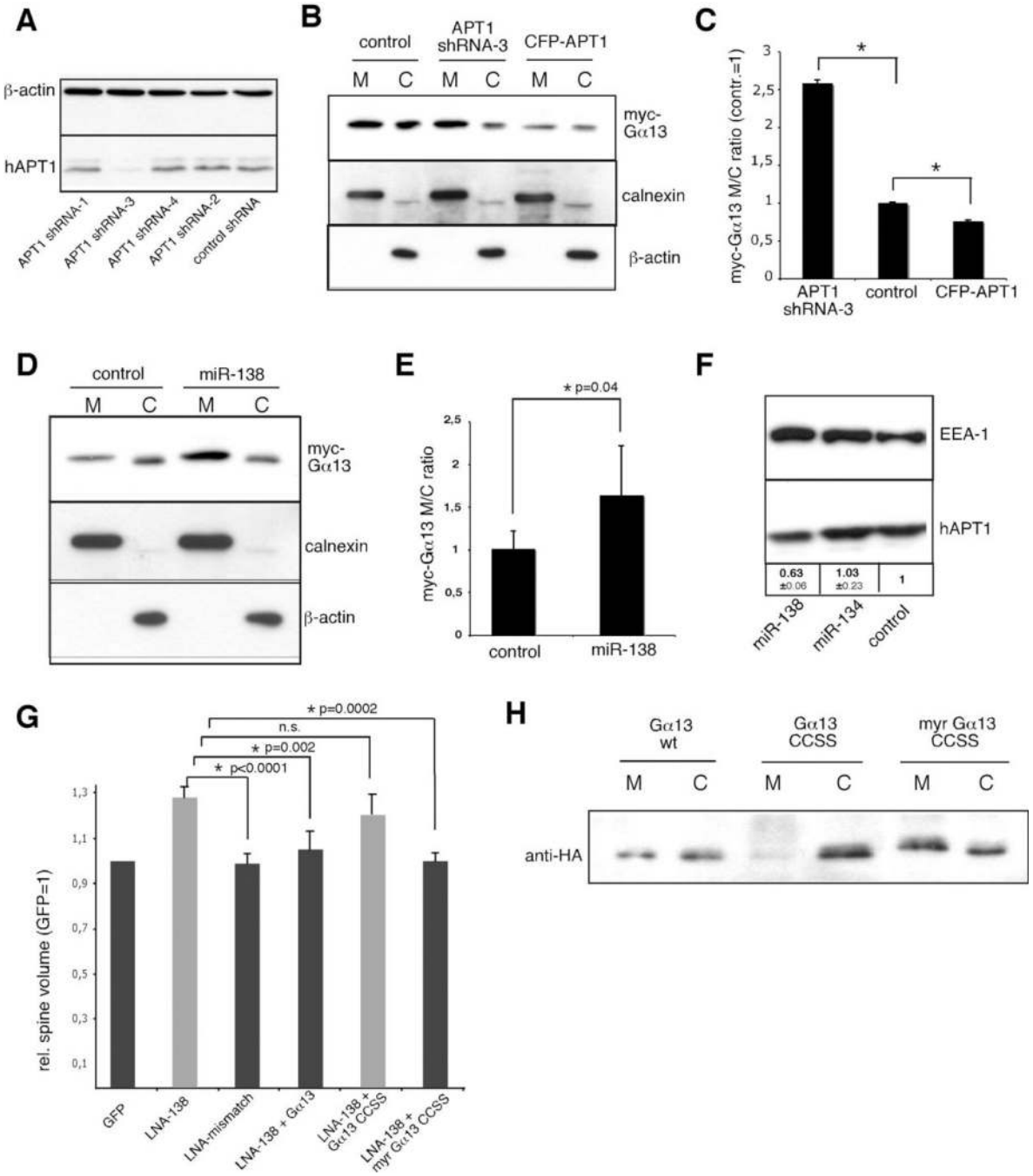

Figure 8. miR-138 regulated membrane-association of Gα13 is required for the control of dendritic spine size

A) Western blot of total lysates from HEK293 cells transfected with control shRNA or APT1 shRNA 1–4 using anti-β-actin (top) or anti-APT1 (bottom) antibodies. A representative blot is shown (n=3). Note that only the APT1 shRNA-3 target site is conserved in human and rat.

B) shRNA-mediated knockdown of endogenous APT1 increases the fraction of membrane-bound myc-Gα13 in HEK293 cells. Western blot of membrane (M) or cytosolic (C) lysates expressing myc-Gα13 together with APT1 shRNA-3 or a control shRNA using anti-myc (top), anti-calnexin (middle) or anti-beta-actin (bottom) antibodies.

C) Quantification of signals obtained by Western blot (Fig. 8B). *p<0.05 (n=3; pairwise Student's t-test).
D) Expression of miR-138 increases the fraction of membrane-bound myc-Gα13 in HEK293 cells. Western blot of membrane (M) or cytosolic (C) lysates expressing myc-Gα13 with or without synthetic miR-138 duplex (40 nM) using anti-myc (top) anti-calnexin (middle) or anti-β-actin (bottom) antibodies.
E) Quantification of signals obtained by Western blot (Fig. 8D). *p<0.05 (n=4; pairwise Student's t-test).
F) Expression of miR-138 decreases endogenous APT-1 protein levels in HEK293 cells. Western blot of whole cell lysates transfected with miR-134, miR-138 or control duplex RNA (10 nM) using anti-APT-1 (top) or anti-β-actin (bottom) antibodies. Quantification of independent blots is shown at the bottom (n=3; control duplex RNA = 1). Note the modest reduction in endogenous hAPT1 protein levels due to low co-transfection efficiency of miR-138 duplex RNA (ca. 50–60%).
G) Expression of membrane-targeted Gα13 rescues spine enlargement caused by miR-138 inhibition. Rat hippocampal neurons (10 DIV) were transfected with the indicated LNA oligonucleotides (100 nM) together with Gα13 expression constructs (250 ng/ml each). Values were normalized to the GFP-only condition and represent the mean ± S.D. (n=3; at least 1800 spines from 18 neurons). p=0.019 (ANOVA). P-values of pairwise Student's t-tests are indicated.
H) Expression levels and subcellular distribution of Gα13 variants. Western blot of membrane (M) or cytosolic (C) lysates from HEK293 cells expressing the indicated Gα13 mutants.